Quantum Yield Regeneration: Influence of Neutral Ligand Binding on Photophysical Properties in Colloidal Core/Shell Quantum Dots

Yi Shen,[†] Rui Tan,[†] Megan Y. Gee,[†] and Andrew B. Greytak*[,†,‡]

[†]Department of Chemistry and Biochemistry and [‡]USC Nanocenter, University of South Carolina, Columbia, South Carolina 29208, United States

ABSTRACT This article describes an experiment designed to identify the role of specific molecular ligands in maintaining the high photoluminescence (PL) quantum yield (QY) observed in as-synthesized CdSe/CdZnS and CdSe/CdS quantum dots (QDs). Although it has been possible for many years to prepare core/shell quantum dots with near-unity quantum yield through high-temperature colloidal synthesis, purification of such colloidal particles is frequently accompanied by a reduction in quantum yield. Here, a recently established gel permeation chromatography (GPC) technique is used to remove weakly associated ligands without a change in solvent: a decrease in ensemble QY and average PL lifetime is observed. Minor components of the initial mixture that were removed by GPC are then added separately to purified QD samples to determine whether reintroduction of these components can restore the photophysical properties of the initial sample. We show that among these putative ligands trioctylphosphine and cadmium oleate can regenerate the initial high QY of all samples, but only the "L-type" ligands (trioctyphosphine and oleylamine) can restore the QY without changing the shapes of the optical spectra. On the basis of the PL decay analysis, we confirm that quenching in GPC-purified samples and regeneration in ligand-introduced samples are associated chiefly with changes in the relative population fraction of QDs with different decay rates. The reversibility of the QY regeneration process has also been studied; the introduction and removal of trioctylphosphine and oleylamine tend to be reversible, while cadmium oleate is not. Finally, isothermal titration calorimetry has been used to study the relationship between the binding strength of the neutral ligands to the surface and photophysical property changes in QD samples to which they are added.

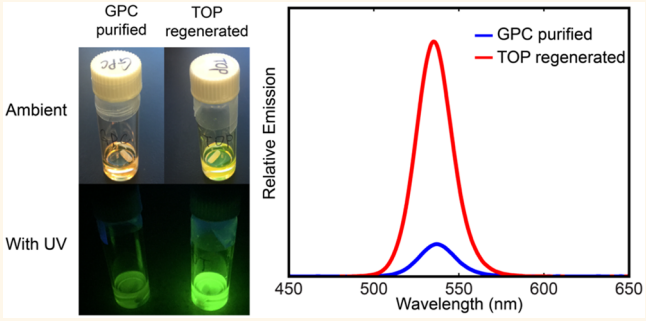

KEYWORDS: CdSe · core/shell quantum dots · quantum yield · enhancement · quenching · time-resolved photoluminescence · ITC

As a result of their electronic structure, colloidal semiconductor quantum dots (QDs) exhibit size-tunable absorption and emission spectra,[1] large molar extinction coefficients,[2,3] two-photon excitation cross sections,[4,5] and high photostability[6,7] compared to most molecular fluorophores. These properties have led to intense interest in QDs as light emitters in bioimaging[5,7−10] and display[11] applications and as light absorbers in solar cells[12−17] and focal plane arrays.[18] However, a limitation in many of these cases is the nonradiative decay rate, which competes with light emission or charge transfer.[19] Nonradiative decay is manifested in less-than-unity quantum yields in ensemble samples and in fluorescence intermittency (blinking) in single-particle measurements.[20−24] Whereas the radiative rate is largely controlled by the delocalized band-edge electronic states,[25−27] nonradiative decay rates can depend sensitively on the interfacial structure.[28,29] In particular, the surfaces are typically populated by exchangeable ligand layers, and numerous studies have examined the ability of ligand exchange to enhance or quench QD photoluminescence (PL).[22,28,30−35]

Core/shell nanostructures, in which a material with a larger bulk band gap encapsulates the core, are a highly effective way to create QDs with lower nonradiative decay rates. As such a higher ensemble quantum yield (QY)[36] and higher on-time fractions among single dots can be achieved.[22,33] Indeed, it is possible to routinely achieve

* Address correspondence to greytak@sc.edu.

Received for review January 29, 2015 and accepted March 9, 2015.

Published online March 09, 2015
10.1021/acsnano.5b00671

near-unity QY in the best-represented material systems such as CdSe/CdS.[33,37] One effect of a shell is to isolate the excited state from the surface by decreasing the wave function overlap with surface states. It is notable that even in samples with shells only a few monolayers thick, in which the excited states are clearly not isolated from the surface, a very high QY can be achieved (for example at the conclusion of QD synthesis).[33] This demonstrates that molecular surface termination can be achieved in which almost no intergap states or resonant excitations are present. As-synthesized colloidal QD samples typically or inherently contain large concentrations of molecules that could coordinate the surface.[38] However, applications almost universally require purification and/or surface modification of as-synthesized QDs. Purification methods have frequently been seen to decrease QY[22,33,39,40] and also to decrease ligand populations.[40−42] It is essential to understand whether the changes in QY are reversible, how ensemble QY and decay profiles depend on ligand occupation, and the conditions under which surface structures that support high QY can be maintained or restored.[43]

Photophysical studies involving the effect of ligands on QDs have recently been reviewed.[35] Previous reports have largely focused on intraband relaxation,[44−46] on molecules that act as quenchers,[32,47−50] on core-only QDs,[31,51−55] or have not been accompanied by the analytical tools to assess the extent of binding as an independent variable controlling decay rates.[56] Mulvaney's group has studied the effects of Lewis bases and other ligands on radiative recombination in CdSe core-only QDs.[31] Ginger's group has studied PL quenching in CdSe-based core and core/shell QDs upon introduction of ligands,[32,47] while PL enhancement in QDs has been observed with thiol-bearing ligands[57,58] and amine-bearing ligands[30,47,59−61] that are not present in the synthetic mixture. However, until now the effect of putative ligands present in as-synthesized core/shell QDs that display high QYs has not been studied.

We recently described[40] the use of size-exclusion chromatography with a polystyrene stationary phase (gel permeation chromatography, GPC) to separate natively capped colloidal QDs from small molecules in organic solvents. This has the effect of removing impurities and weakly bound ligands, including phosphines, phosphine oxides, and primary amines, enabling the preparation of QDs with surfaces bearing a low and consistent number of metal carboxylate equivalents.

In the present study, we take advantage of GPC purification of core/shell QDs to explore the role of neutral ligands in maintaining high QY. In particular, we measured the ensemble QY and PL decay profile of oleate-capped core/shell QDs before and after GPC and then upon reintroduction of putative ligands that were present in the growth solution. Historically, PL decays of QDs recorded at low excitation densities have frequently displayed multiexponential behavior, which has been interpreted as a consequence of a distribution of trapping rates inhabited by different QDs in the ensemble.[62−64] Through lifetime analysis, it may be possible to distinguish between different modes of QY reduction and regeneration in QDs with different densities of unoccupied ligand binding sites. For example, a given reduction in the ensemble QY could be brought about by a reduction in QY among all QDs in the sample, leading to a reduction in lifetime among all decay components. Another possible mechanism would be selective quenching of a portion of the QDs, leading to an increase in the relative amplitudes of short-lifetime decay components. The former case might be expected if nonradiative recombination in purified QDs occurs *via* a large number of traps associated with vacant surface sites, while the latter case might be expected if ligand occupation modulates stochastic quenching processes such as those responsible for fluorescence intermittency in single QDs.[20,32,65]

In analyzing the response of QDs to the introduction of neutral ligands, it is essential to know whether changes in ligand concentration lead to irreversible structural changes in the QDs. Therefore, we have also studied the reversibility of the QY regeneration process. Additionally, it is valuable to be able to evaluate the actual extent of ligand coverage on the QD surface: in other words, what fraction of the added ligand is interacting with the QD surface at one time. Changes in the NMR line shape between bound and free ligands may not be resolvable in the case of rapidly exchanging ligands, and changes in the effective diffusion constant as measured by diffusion-ordered NMR spectroscopy (DOSY)[40,66] may be difficult to detect for low bound-ligand mole fractions. Here, we used isothermal titration calorimetry (ITC)[55,67−71] to differentiate the extent of ligand binding in QD samples exposed to phosphine, primary amine, and phosphine oxide ligands in an organic solvent.

RESULTS AND DISCUSSION

Quantum Yield Decrease upon Purification. We chose four types of CdSe-based core/shell QD materials that we synthesized by a selective ionic layer adhesion and reaction (SILAR) method.[33,72] The effect of ligand occupation on QY in QDs with either pure CdS or CdZnS alloy shells and with different shell thicknesses was studied. **CdSe/CdS_1** and **CdSe/CdZnS_1** are the thin shell samples (1.6 monolayer equivalent shell thickness), and **CdSe/CdS_2** and **CdSe/CdZnS_2** represent thicker shells (4 monolayer equivalent shell thickness). The formation of the shell was monitored by withdrawing a small aliquot and diluting into toluene; the aliquots were characterized by UV−vis absorption

TABLE 1. Characteristics of QD Samples Used before and after GPC Purification

	CdSe/CdZnS_1	CdSe/CdZnS_2	CdSe/CdS_1	CdSe/CdS_2
core radius (nm)[a]	1.52	1.52	1.65	1.65
shell thickness (ML)[b]	1.6	4	1.6	4
absolute QY before GPC[c]	64%	88%	73%	81%
relative QY drop after GPC	−84%	−23%	−70%	−28%
olefin proton to QD ratio drop after GPC[d]	−93%	−94%	−93%	−95%
removal of phosphorus-containing ligand after GPC?	yes	yes	yes	yes

[a] The core radius was estimated by a calibration curve describing the radius as a function of the position of the lowest energy absorption peak.[2,3] [b] "ML" is the abbreviation of monolayer equivalents. [c] The QY of QD samples was measured relative to a rhodamine 590 standard (R590, QY = 99% in ethanol[77]). [d] The ratio was determined by quantitative ^{1}H NMR and UV−vis as described previously.[40]

spectroscopy (Figure S1) and fluorescence emission spectroscopy (Figure S2). The QYs of these samples were recorded after isolation of the particles by one cycle of precipitation with acetone and redissolution in toluene. As shown in Table 1 and Figure S3, the high QY indicates a complete formation of the shell onto the CdSe core materials.

NMR has been demonstrated as a useful technique for the determination of the presence and interactions between ligands and nanocrystals, especially for ligands with a distinctive signal.[66] As a result, some of the best studied ligands on the QDs fall into two groups, namely, the phosphorus-containing group and the olefin-proton-containing group, which both can be distinguished easily in ^{31}P NMR or ^{1}H NMR spectra. The phosphorus-containing group includes trioctylphosphine (TOP) and trioctylphosphine oxide (TOPO), which are among the solvents used in core synthesis and shell growth, and tetradecylphosphonic acid (TDPA) and its cadmium salt (CdTDPA), which can be used as the Cd precursor during CdSe core preparation. The olefin-proton-containing species are frequently introduced in the shell growth process: for example, cadmium oleate (CdOA) and oleic acid (OA) as the Cd precursor, and oleylamine (OAm) and octadecene (ODE) as solvents.[73] Here, we used ^{31}P NMR and quantitative ^{1}H NMR to characterize the QD samples before and after the purification by GPC, which has been shown as a highly efficient and reproducible way to purify QDs[40] and oxide nanocrystals.[74] Figure 1 shows the NMR spectra of **CdSe/CdZnS_1** before (Figure 1A) and after (Figure 1B) the GPC purification in toluene. In Figure 1A, four sharp signals representing free TOPO (53.48 ppm), TDPA (42.34 ppm), dialkylpyrophosphonate (28.74 ppm), and TOP (−32.34 ppm) can be identified in the ^{31}P NMR spectra.[72,75,76] A large amount of olefin-containing species (4.8−5.8 ppm, ~3950 olefin protons per QD) are represented in the ^{1}H NMR.[40] However, after the GPC purification, all the phosphorus-containing ligands have been removed completely and the total amount of olefin proton has significantly decreased (Figure 1B). The rounded shape peak in the olefin region indicates that the only remaining olefin ligands are strongly interacting with

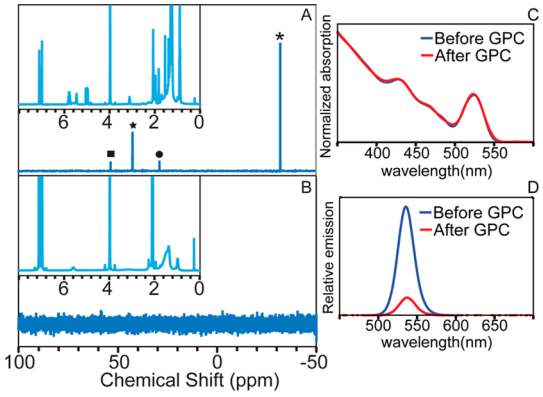

Figure 1. Characterization of CdSe/CdZnS_1 sample before and after the GPC purification. The ^{31}P NMR spectra of the sample before the GPC purification (A) and after the GPC purification (B) with the ^{1}H NMR shown in the insets. The marks in (A) indicate the peaks associated with the phosphorus-containing molecules that are removed during the purification. (C) Absorption spectra of the sample (normalized to 365 nm) before and after the purification. (D) Relative emission spectra of the sample (normalized to the absorption of the excitation wavelength, 365 nm) before and after the purification.

the QD surface; we attribute this to an ionic (X-type) binding mode of residual oleate.[75] The other three QD samples show similar NMR responses to purification (Figure S4), and all the results have been summarized in Table 1.

Concurrent with the removal of the neutral ligands, the emission intensities of the particles all decrease upon GPC purification. The relative QY of **CdSe/CdZnS_1** decreased by 84% after GPC with no shift in the absorption and emission spectra, which implies that the decrease of brightness is not associated with etching/aggregation (Figure 1C,D). As discussed below, we attribute the QY decrease to an increase in nonradiative decay associated with the removal of weakly associating ligands. Similar results can also be observed in the other three samples (Figure S5 and Table 1). Among the four samples, **CdSe/CdZnS_1** (84%) and **CdSe/CdS_1** (70%) samples show the higher emission intensity drop than **CdSe/CdZnS_2** (23%) and **CdSe/CdS_2** (28%) samples, which can be explained by better isolation of the excitons from the surface traps with a thicker shell. Importantly, these changes are

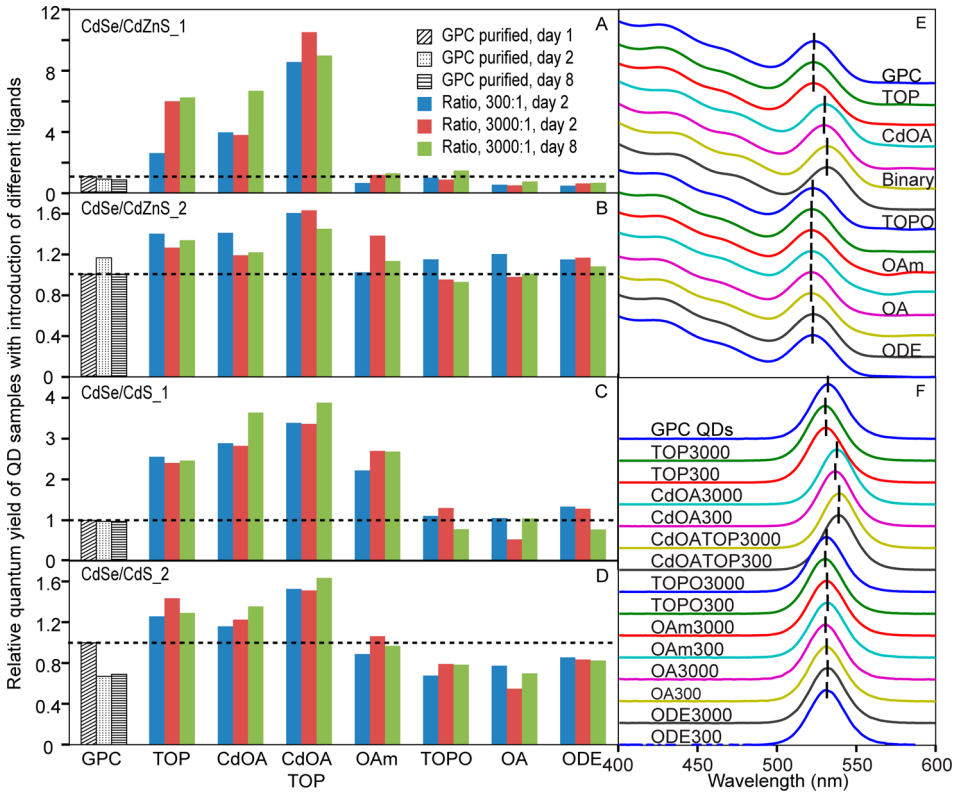

Figure 2. QY regeneration results with introduction of different ligands. (A–D) The relative QY of GPC-purified stock solution and ligand mixing solutions for CdSe/CdZnS_1 (A), CdSe/CdZnS_2 (B), CdSe/CdS_1 (C), and CdSe/CdS_2 (D). All of the results are normalized to the QY of the freshly GPC-purified samples shown with the dashed line. (E) Absorption spectra of the GPC-purified CdSe/CdZnS_1 QDs mixing with different ligands on day 2. Here, the CdOA and TOP mixture is described as binary in short. The labeled curves have a 3000:1 ligand-to-QD ratio, while the curves below have a ratio of 300:1. (F) Emission spectra during the regeneration process for CdSe/CdZnS_1. The label is a combination of the ligand type and ligand-to-QD ratio. The samples are the same as the absorption measurements in (E). Both absorption and emission spectra are normalized to the lowest energy extinction peaks.

brought about in the absence of any change in solvent or precipitation of the QDs or introduction of protic or nucleophilic species that are known to displace ligands from QD surfaces.[41,42,53] These well-characterized and isolated QDs therefore provide a good model system to study whether the above process is reversible and which ligands are responsible for the initial high QY.

QY Regeneration by Introduction of Neutral Ligands. After the purification, the QDs were immediately transferred into a nitrogen-filled glovebox to suppress oxidation. According to the NMR spectra recorded before and after the GPC process, the ligands that were removed by GPC include OA, CdOA, OAm, and ODE from the olefin-proton-containing group and TOP, TOPO, TDPA, and CdTDPA from the phosphorus-containing group. We sought to determine whether reintroduction of these species to the system could restore the QY. In order to avoid possible ligand exchange reactions, we chose not to include TDPA and CdTDPA among the neutral binders studied in this work since phosphonic acid is known to displace oleate from the surface of CdSe QDs.[78] Therefore, we have introduced the first six ligands individually, as well as a mixture of TOP and CdOA, back to QD solution with two different ligand-to-QD ratios (300:1 and 3000:1). The lower number is intended to be roughly comparable to the total number of surface sites per QD, while the larger number represents an excess.[38,47,55] After mixing the ligands and the purified QDs for a certain period of time (1 day and 7 days), the QY of each of the samples was measured. The relative QY among QDs with similar absorption spectra, emission spectra, and solvent can be measured with high precision, and therefore we report this value. In particular, we measured the QY changes during the observation period by comparing to an as-synthesized QD solution reference. As shown in Figure 2 (left column), the emission intensities of most of the GPC-purified QD solutions decreased upon storage in the glovebox for the longer period of time, though for sample **CdSe/CdZnS_2**, the QY increased slightly after 1 day of storage. The changes observed in purified samples during storage in dilute solution in the absence of ligand addition could be due to slow re-equilibration of the surface-bound and/or free metal oleate, and these samples serve as a control for the response to ligand addition.

We found that reintroduction of selected ligands resulted in a significant increase, or "regeneration", of QY in all samples tested. When we compare the response to introduction of the putative ligands, the

QY is enhanced when TOP and CdOA are introduced in all four samples. The combination of TOP and CdOA always shows the greatest amount of QY regeneration, which indicates that these two ligands are increasing the QY in a complementary manner. OAm can regenerate the QY in CdSe/CdS samples (especially **CdSe/CdS_1**), but the QY did not significantly increase with the presence of OA, ODE, or TOPO. For example, as shown in Figure 2A, compared to the freshly GPC-purified **CdSe/CdZnS_1** sample, the QY increased 6-fold when the higher amount of TOP is introduced and remained at a level close to the initial QY before GPC purification for the 7-day measurement period. The binary ligand system shows the highest amount of QY regeneration, up to ~12 times the GPC-purified control at the same time point for **CdSe/CdZnS_1** (the QY of the GPC stock solution decreased 16% after 1 day of storage). The QY regeneration of the thin-shell QDs is much higher than that of the thick-shell samples, which mirrors the observation of a smaller decrease in QY after the GPC purification. We did not observe a large difference in response at the two different ligand-to-QD ratios, which indicates that the surface has been completely saturated at the lower concentration of neutral ligands.[31] All the ligands behave similarly for CdZnS and CdS shells except when OAm is introduced. When OAm is introduced to CdSe/CdZnS QDs, the QY does not increase; however, the QY does increase significantly when OAm is added to CdSe/CdS QDs. For **CdSe/CdS_1**, the response to OAm is close to that of TOP. One interpretation of the role of "L-type" ligands in maintaining QY is that ligand orbitals mix with interfacial localized states to move them outside of the band gap.[35,79,80] In this interpretation, band-edge quantum-confined states are minimally affected. CdZnS has a larger bulk band gap than pure CdS, and so the interaction between OAm and the surface trap states is not strong enough to move the states outside of this larger shell band gap. The influence of relative binding strength on QY will be further addressed below.

Figure 2E and F show the absorption and emission spectra of GPC-purified **CdSe/CdZnS_1** QDs after mixing with different ligands as described above. An important goal of our study is to detect differences in structure and composition between initially prepared and purified QD samples that could be responsible for QY changes. Consequently it is important to check whether the initial absorption and emission spectra, which did not change significantly on purification, are maintained upon reintroduction of putative ligands. Both absorption and emission spectra remain constant with the introduction of the L-type ligands we investigated; however, in the case of CdOA, which behaves as an electrophilic "Z-type" ligand,[53] a significant red shift is observed. We observed similar results for pure CdS shell samples (Figure S6). This indicates that the decreases in QY of the QDs after purification, which occurred without red or blue shift, are more directly related to the removal of the L-type ligands (TOP or OAm) than CdOA even though a higher coverage of Cd has also been shown to increase the brightness of CdSe and CdSe/CdS samples in published reports.[53,81] The red shift can also be observed when introducing CdOA to the QDs sample before the GPC purification, which confirms that the red-shift response is not a consequence of the GPC purification (Figure S7).

Lifetime Analysis by Time-Resolved Fluorescence Spectroscopy. To gain additional insight on possible mechanisms for quenching and restoration of QY as a function of ligand concentration, we measured the PL decays of stirred QD samples in anhydrous toluene under 368 nm pulsed excitation, which is similar to the excitation wavelength we used for the relative QY measurements (365 nm). Since thin-shell QD samples display a larger response to the introduction of the ligands, we will focus on **CdSe/CdZnS_1** and **CdSe/CdS_1** samples in this discussion; the thick-shell QD samples **CdSe/CdZnS_2** and **CdSe/CdS_2** behaved similarly (Figure S8). Data collected over 200 ns revealed multiple lifetime components (Figure 3A,B insets), including a long-lived tail with an apparent lifetime of >50 ns. Previous reports of PL decays on QD samples with near-unity absolute QY[33,37,82] and reported decays of single QDs in the "on" state[24] support a radiative recombination lifetime $k_r^{-1} \approx 20-30$ ns for CdSe-based QDs similar to those described here. Accordingly lifetime components are likely a result of trapping/detrapping processes.[25,64] In order to focus on the principal reasons for changes in ensemble QY, we chose to focus on the first 50 ns, which contain >90% of the light emitted (Figure 3A,B). The lifetime curves of the samples mixed with TOPO, OAm, and TOP will be compared with the samples before and after the GPC purification. Since the introduction of CdOA results in a change in the band-edge electronic structure of the sample based on the absorption spectrum, the radiative recombination rate is not expected to be the same as in the other samples. Therefore, the lifetime result of CdOA cannot be directly compared to the above three ligands (see Figure S9). Introduction of the ODE control resulted in only small changes in the decay traces (Figure S10).

In general, the trend of the lifetime results is similar to the observation of the QY changes, where the samples with higher QYs have longer average lifetimes. The decays shown in Figure 3A,B show a relatively constant slope of the logarithm of intensity with respect to time in a window of ~20−50 ns, and this slope was similar among samples with different ensemble QYs. However, samples with lower QYs displayed significantly greater intensity loss within the first 10 ns. This trend is more clearly apparent when the decay traces are normalized at 30 ns to emphasize

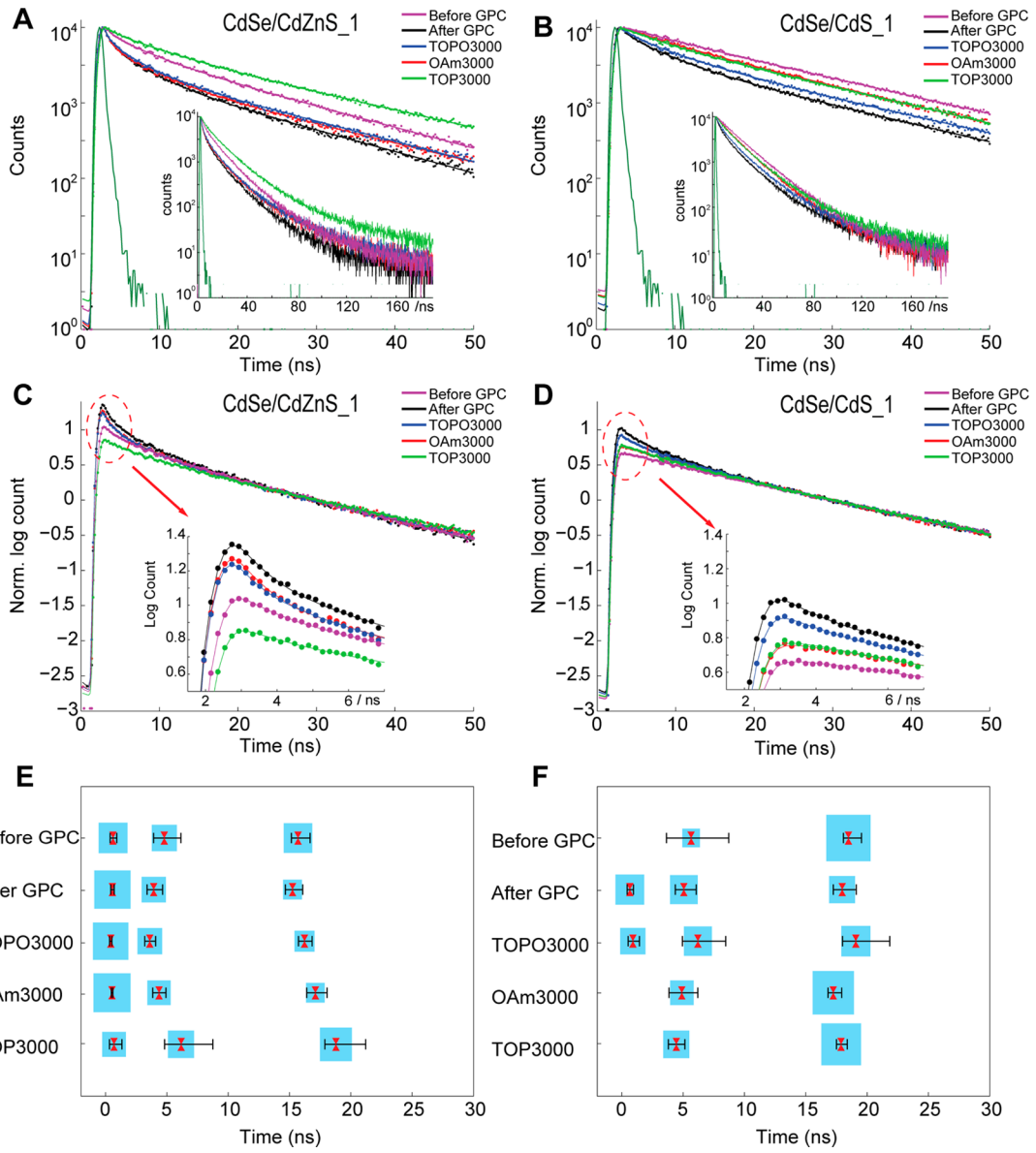

Figure 3. Comparison of fluorescence lifetime decays for CdSe/CdZnS_1 (A) and CdSe/CdS_1 (B) core/shell QDs before/after GPC purification and subsequently mixed with different ligands, focused on the first 50 ns. Data collected over 200 ns are shown in the insets. (C, D) Corresponding lifetime decays normalized at 30 ns; insets show detail. Lines are reconvolution fits. (E, F) Charts displaying lifetime values and corresponding amplitudes for reconvolution fits of PL decay traces for CdSe/CdZnS_1 (E) and CdSe/CdS_1 (F). The weighted amplitudes are represented by the areas of the blue squares, while the lifetime values are indicated by red marks at the center of each square. Error bars indicate the uncertainty of each lifetime component as obtained by support plane analysis with a confidence limit of 90%.

differences in decay rate at earlier times (Figure 3C,D and insets therein). After GPC purification, QY regeneration (as observed upon introduction of TOP in both samples and OAm in **CdSe/CdS_1**) is accompanied by reduction, but not complete elimination, of the accelerated decay at early times.

Analysis of rate dispersion in ensemble QD samples and time evolution of decay rates in single-QD photon counting experiments have supported an interpretation of rate dispersion as being primarily or entirely inhomogeneous in QD samples, the result of subpopulations with varying decay rates.[24,63] Subpopulations with lower QYs are expected to display shorter lifetimes because of elevated nonradiative decay rates. In this case, it may be possible to constrain models of nonradiative decay by decomposing the observed decays into several lifetime components. We employed a reconvolution fit with multiple decay lifetimes to analyze the decays within the first 50 ns. Uncertainty in the lifetime values was examined with support plane analysis[83] (a detailed description of the analysis is available in the SI). With this analysis, the longest lifetime approximates the decay seen in the ~15−25 ns window, while the shorter lifetimes describe the rapid decay seen at early times. By analyzing the rates and amplitudes of the lifetime components, we sought to

distinguish whether quenching in GPC-purified samples and regeneration in ligand-introduced samples are associated chiefly with changes in lifetime among all lifetime components or with changes in the relative population fraction of QDs with different decay rates, as assessed from the amplitudes of the short and long lifetime components of the fit.

In the case of thin alloy shells (Figure 3E), we found that a three-component lifetime fit was statistically supported by the data, while the bright QD samples with pure CdS shell (**CdSe/CdS_1** before GPC, with TOP3000 and with OAm3000) required only two components (Figure 3F). We found that the change in QY between the samples before and after GPC, and between GPC and QY regenerated samples, is accompanied by a change in the amplitude of the lifetime components, with little change in the lifetime value. For example, the amplitude average lifetime of **CdSe/CdZnS_1** after the GPC purification is 3.77 ns; after mixing with TOP, the lifetime increases to 10.49 ns (we report amplitude average lifetimes because they are nominally proportional to the steady-state fluorescence intensity[84]). The values of the component lifetimes change no more than 30%, but the amplitude ratio between the shortest and longest lifetime components increases by a factor of 6.7. Similar results can be observed in comparing GPC-purified QDs to the initial samples prior to GPC (see Table S1 for detailed lifetime values and exponential amplitudes). Thus, the reduction in QY upon removal of L-type ligands appears to be driven primarily by a large increase in decay rate among a subset of the QDs.

We can use the PL decay profiles to consider possible models for quenching in QDs with vacant L-type ligand sites. One model is to consider each vacant site to contribute a similar nonradiative decay rate, in an additive manner.[35,47] In this case, the distribution of decay rates in the purified samples will reflect the distribution in the number of vacant sites per QD. But because each QD presumably contains numerous binding sites for L-type ligands[47,55] and nearly all are vacant following GPC purification, it would seem improbable that a significant fraction of the purified QDs would have zero vacant sites and thus remain unquenched. We therefore rule this model out. A second model considers a stochastic quenching process, such as the formation of charged QDs leading to Auger recombination,[20] whose probability is tuned by ligand coverage. In this model, ligand coverage does not significantly affect the component lifetimes, but rather tunes the population fraction that is in a bright or quenched configuration at a given time, in a manner analogous to the fluorescence intermittency seen in single-particle studies.[85] A third possibility is that the most significant changes in QY arise from vacancies at a subset of L-type ligand binding sites that occur rarely enough that some QDs in the ensemble lack such sites and do not experience quenching at low ligand concentration. Measurements that link structure and QY among individual QDs[86] may be of value in distinguishing among these models. Spectroscopic techniques such as transient absorption, upconversion PL decay measurements that can more precisely resolve rapid decay processes, and multiple-pulse experiments have been applied to the analysis of QD radiative and nonradiative decay.[35,62,63,87,88] It is clear from the results presented here that the ensemble QY, average decay rate, and rate dispersion of QDs change in response to ligand concentration. Thus, spectroscopic analyses must ideally be performed on samples with well-specified ligand populations and concentrations if the results of such studies are to be compared or applied to new systems.

Time Evolution of QY Regenerated Samples. While the results in Figure 2 show that QY regeneration upon introduction of excess ligands can be maintained over a period of at least a week, we sought to study the time evolution of QY and PL decay profiles in greater detail. We focused on the thin-shell QD samples with introduction of 3000 equiv of TOP, a treatment that improved the ensemble QY in all cases. As shown in Figure 4A and B, the brightness of the QD samples can be fully regenerated to the level prior to GPC purification after mixing with TOP for 1 h, which suggests that the high QY of the sample before the purification is due to the presence of neutral ligands such as TOP. On the basis of the time evolution of the relative QY, the alloy shell sample requires a longer period of time to reach equilibrium; in this case the sample at 5 min is only halfway through its full regeneration, whereas at 5 min the pure CdS shell sample is close to its maximum brightness. The high QY in the TOP-introduced **CdSe/CdZnS_1** sample can be maintained for 7 days, but there is a decrease in QY with the TOP-introduced **CdSe/CdS_1** sample after 1 day. As shown in Figure 4C and D, the lifetimes of each component for the TOP-introduced samples are fairly similar at different waiting times (see Table S2 for fit parameters). These results are consistent with changes in the relative population fraction of QDs with different decay rates driving QY regeneration in the GPC-purified samples.

Reversibility of QY Regeneration. One concern is whether changes in ligand concentration lead to irreversible structural changes in the QDs. To investigate the reversibility of the regeneration process, a second round of GPC was used to repurify the QY-regenerated thin-shell QD samples, subsequent to introduction of CdOA, TOP, or OAm. By comparing the absorption and emission spectra before and after the second purification, we can detect irreversible changes in size or shape associated with changes in ligand concentration.

As shown in the initial QY regeneration results, when CdOA is introduced into both **CdSe/CdZnS_1** and **CdSe/CdS_1** samples, there is a red shift in the absorption spectra. As shown in Figure 5A,B, they did

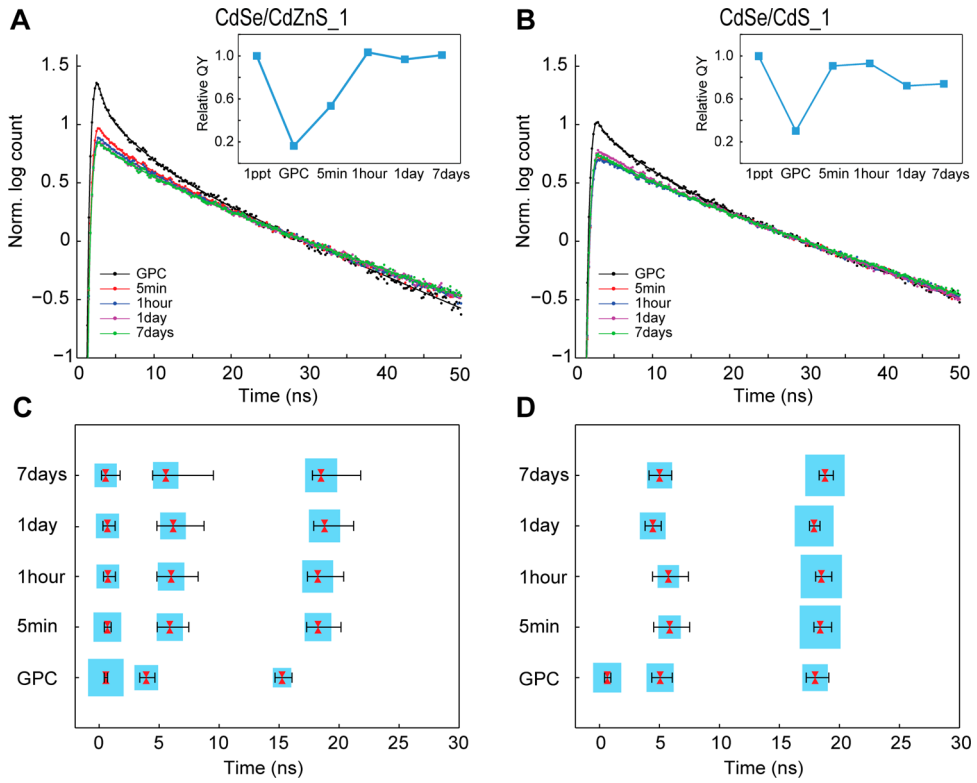

Figure 4. Fluorescence lifetime decays for CdSe/CdZnS_1 (A) and CdSe/CdS_1 (B) core/shell QDs after GPC purification and then at various times after the introduction of TOP, normalized at 30 ns. Changes of relative QY are shown as insets. Here, the sample before GPC purification is described as "1ppt" in short. (C, D) Reconvolution fits of the corresponding decays gave the weighted amplitudes (area of blue squares) and lifetimes of each component (red marks at the center of each square) for CdSe/CdZnS_1 (C) and CdSe/CdS_1 (D) mixed with TOP over time. The uncertainty in each lifetime component was obtained by support plane analysis with a confidence limit of 90%.

not shift back after the second GPC purification process, which indicates that the regeneration process with CdOA is not reversible. The small red shift in the **CdSe/CdS_1** sample on introduction of CdOA is analogous to that seen when CdOA is used as a Cd precursor in shell growth, but the irreversible nature could indicate some surface reconstruction.[72] When CdOA is added to the **CdSe/CdZnS_1** sample, a larger red shift is observed, and one possible reason is a cation exchange reaction between Zn from the shell and CdOA in the solution.[89−91] To confirm this, purified **CdSe/CdZnS_1** treated with CdOA solution or pure toluene was precipitated, and the supernatant portions of these two samples were digested and characterized by inductively coupled plasma-mass spectrometry (ICP-MS). As shown in Figure 5C, a much higher amount of Zn is observed in solution when CdOA is introduced. The total amount of excess Zn detected in the supernatant corresponds to 25.3% of the Zn equivalents introduced during shell synthesis; this suggests that at least 25.3% of the Zn in the shell has been replaced by Cd. One interesting observation is that for GPC-purified **CdSe/CdS_1**, after treatment with a large excess of CdOA, a subsequent GPC purification found a significant portion of the sample to be retained on the GPC column. Interactions between

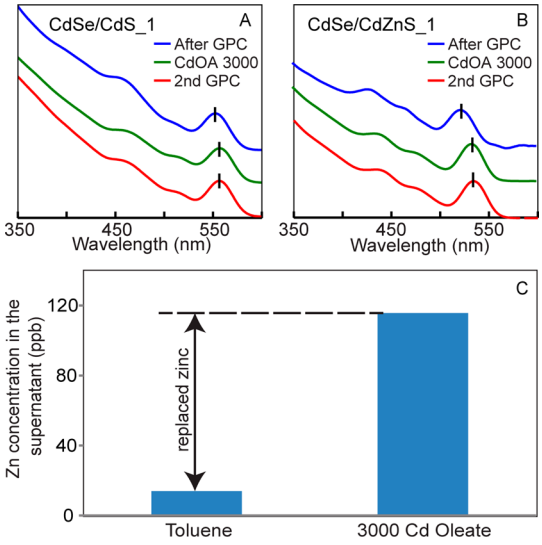

Figure 5. Reversibility test of CdOA. (A, B) The absorption spectra before and after the introduction of CdOA and after the second GPC purification for CdSe/CdS_1 (A) and CdSe/CdZnS_1 (B). (C) ICP-MS analysis of the Zn content in digested supernatant of GPC-purified CdSe/CdZnS_1 sample mixed with toluene or with 3000 equiv of CdOA solution.

polystyrene GPC media and metal-rich samples have been reported in other systems.[92] We have observed similar results previously when attempting to purify

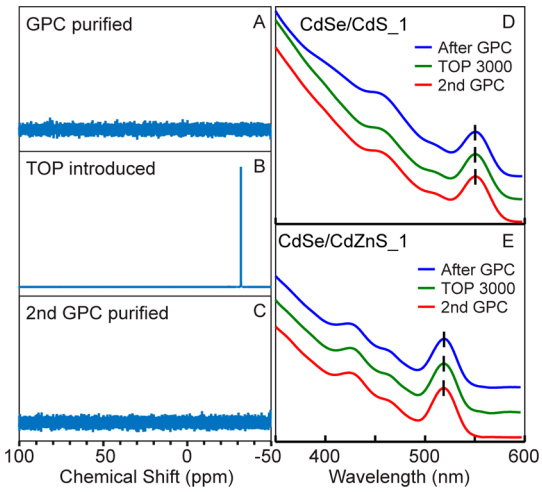

Figure 6. Reversibility test of TOP. ^{31}P NMR spectra before (A) and after (B) the introduction of TOP and after the second GPC purification (C) for the GPC-purified CdSe/CdS_1 QDs. The absorption spectra during the process described above for CdSe/CdS_1 (D) and CdSe/CdZnS_1 (E).

QDs synthesized under highly metal-rich conditions, which is consistent with CdOA adhesion to the CdSe/CdS QD surface in the present case.

On the other hand, Figure 6D and E show that, during introduction and removal of TOP, both CdSe/CdS and CdSe/CdZnS QD samples maintain their absorption features. This suggests that TOP does not change the effective size or size distribution of the quantum-confined band-edge states (there is an increase in relative absorption in the UV range, which may be associated with changes in higher energy excitations). After the second GPC purification, NMR confirms that TOP can once again be completely removed from the system and the absorption spectrum remains constant (Figure 6A–C and Figure S11). On the basis of these results, we believe that the regeneration process with TOP is reversible. Similar results can also be observed with OAm, where the α-H disappeared after the second GPC purification (Figure S12). According to the emission spectra, the QY decreased after removing TOP by the second GPC purification, but it remained higher than the first GPC-purified sample. This result suggests that the regeneration process with TOP might not be completely described as a simple adsorption reaction and the QD surface may reconstruct with the help of the introduced L-type ligands. Previous reports have identified a role of L-type ligands in displacing metal oleate from CdSe QD surfaces at high concentration.[53] Here, we also attempted to measure the oleate population after the second GPC purification, but due to the aggregation of the particles during the phase change process when switching to deuterated solvent (the absorption spectra changed and emission intensities significantly decreased after removal of the solvent and redissolution process, Figure S13), we were unable to obtain consistent results based on NMR and absorption spectra.

Isothermal Titration Calorimetry Comparison of TOPO, TOP, and OAm Ligand Addition. On the basis of our results above as well as previous literature reports, L-type ligands (including TOP, TOPO, and OAm) can reversibly attach to and detach from the QD surface.[31,38,55] However, as shown in our regeneration and lifetime studies, not all of these ligands contribute directly to the photophysical property changes in QDs. Ligand/QD interaction is known to influence the energy levels and occupation of interfacial states, affecting electron and hole trapping rates and intraband decay rates.[35] The effect of a certain total ligand concentration will depend on the adsorption isotherm and on the effect of such binding on the interfacial states. It is desirable to have an independent measurement of the extent of binding so that these factors can be distinguished. NMR has been proven to be a powerful technique for the determination of the interactions between ligands and the nanocrystal surface. Diffusion-ordered NMR analysis has been employed specifically to characterize the bound and free ligand population on QDs in previous work.[40,66] However, in this study, we did not observe any significant difference in diffusion constant measured by DOSY (Figure S14), T_1 measurement on ^{31}P, or NOE response on ^{1}H spectra with selective saturation on the ^{31}P resonance (data not shown) upon introduction of GPC-purified QDs to TOP or TOPO solutions. Both behaved similarly to free ligand controls in these NMR experiments. These results suggest a fast dynamic adsorption/desorption equilibrium, where the bound ligands are exchanging rapidly with the excess of unbound ligands in the solution.[93] Therefore, we employed isothermal titration calorimetry to detect and characterize the binding between the neutral ligands and QDs. Although widely used in biochemistry, ITC has only recently begun to be applied to nanoparticles to assign parameters for multiple binding problems.[55,69,71,94] In this study, we titrated the same amount of TOPO, OAm, and TOP to the GPC-purified **CdSe/CdZnS_1** sample to measure the heat response. Any response of the system as equilibrium is re-established that has nonzero enthalpy change, such as bond formation upon ligand binding, will generate a heat response. The shape of the heat response over the course of the titration can be used to characterize the equilibrium constant and stoichiometry of reactions, while the sign and magnitude of the signal characterize the associated enthalpy change. Due to the intolerance of the machine toward toluene, anhydrous tetrahydrofuran (THF) has been used as the solvent for this study.

As shown in Figure 7, when TOPO is titrated, the overall heat response is small and no trend can be observed in the integrated curve, which indicates that there is no significant binding between TOPO and the

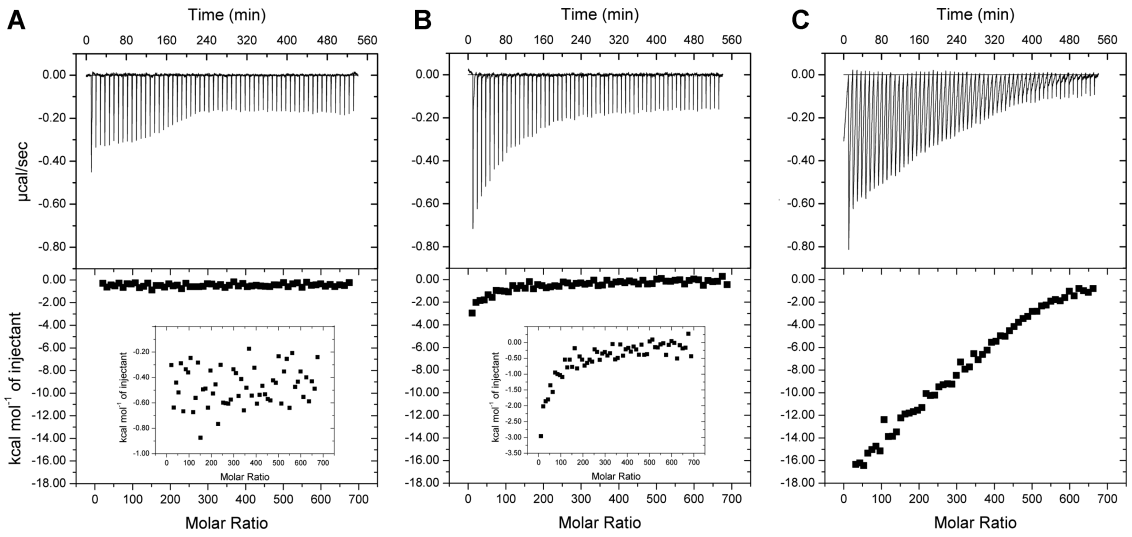

Figure 7. ITC traces for CdSe/CdZnS_1 titrated with TOPO (A), OAm (B), and TOP (C) at the same concentrations. Top panel displays the raw heat per injection, while the bottom panel shows the integrated curves adjusted to the scale for the TOP titration. Insets in bottom panels (A) and (B) show zoomed-in integrated curves for TOPO and OAm titrations, respectively. Ligand-to-solvent reference titrations have been subtracted from the traces shown; solvent-to-solvent and solvent-to-QD runs gave negligible responses.

QDs at these concentrations. The ITC trace for introduction of OAm shows a small exothermic response at low ligand concentration that rapidly saturates. This rapid saturation indicates a high association equilibrium constant. The thermogram was fit with the simple independent identical sites model by varying the number of sites per QD N, equilibrium constant K, and molar enthalpy change ΔH. The best fit was obtained when the number of sites is close to 10, with $K = 2.3 \times 10^4$ M^{-1} and $\Delta H = -27$ kcal/mol. However, since the magnitude of the equilibrium constant K is small and the QD concentration is low, the molar enthalpy change ΔH and the number of sites N are correlated in the fit. In particular, the shape of heat response curves within this model are parametrized by Brandt's c parameter (c = [QD]KN, [QD] is the concentration of the QDs).[67] For data that are characterized by c values smaller than 1 (indicating a small mole fraction of bound ligands out of the total added), the enthalpy change and the number of sites are correlated, but the equilibrium constant K is well constrained. When TOP is introduced, there is a much greater exothermic response than for the reaction with OAm (an overall exothermic heat approximately 14 times more than that of OAm). The greater heat indicates that TOP has a more negative molar enthalpy of binding and/or binds to a greater number of sites per QD than does OAm. As seen in the PL response during QY regeneration, slower kinetics are also observed in the raw heat signal, which does not rapidly return to baseline between injections when TOP is introduced to the **CdSe/CdZnS_1** QDs. The thermogram for TOP cannot be well-fit by a simple independent identical sites model. In order to compare the results for TOP and for OAm, one approach is to consider the difference in ΔH and K that would be required if the number of binding sites per QD is considered to be the same. In this case, a fit with N fixed to 10 reveals $\Delta H_{TOP\_QD}/\Delta H_{OAm\_QD} = 37$ and $K = 4.3 \times 10^3$ M^{-1} for TOP. Despite an apparently larger equilibrium constant for OAm than for TOP, introduction of OAm leads to much less change in QY than TOP, particularly in alloy shell QDs. This could indicate that the ITC signal for OAm corresponds to binding to only a subset of active trapping/quenching sites or that binding of OAm does not sufficiently perturb the energy levels associated with trapping and recombination. However, due to the steric and electronic differences between these molecules, it is highly possible that OAm and TOP bind to different sites on the QD and the number of sites is not the same. The trends we observed in ligand binding strength are consistent with those predicted in Rempel's work for ligands binding to the Se-terminated (0001) surface of wurtzite CdSe.[95] The theoretical value of the binding energy between TOP to wurzite CdS S-terminated (0001) surface is 3.13 eV.[96] If we assume the binding behavior of TOP to the CdZnS alloy shell surface is similar to that for pure CdS, then the total heat response that we observe of about −200 eV/QD (obtained by integrating the response shown in Figure 7C) corresponds to about 60 available sites for TOP per QD. We believe that a more adequate model accounting for interactions among similar and dissimilar ligands is needed to describe such ligand association, dissociation, and exchange reactions more thoroughly, and this could be an important target for future studies. Nevertheless, it seems reasonable to argue,[35] particularly for ligands behaving as σ donors, that a strongly exothermic bond-forming step, leading to a large energy separation between bonding and antibonding orbitals, could

assist in displacing electron traps from within the band gap. The trend of enthalpy change and QY regeneration that we observe supports this argument.

CONCLUSIONS

The maintenance of high PL QY is important to applications of QDs in lighting and displays, bioimaging, and luminescent solar concentrators.[16,17] In optoelectronic devices such as solar cells it is likewise important to passivate interfaces in such a way as to limit nonradiative recombination.[15] Surface-adsorbed molecules (ligands) play at least two roles in the behavior of colloidal QDs: they maintain solubility and suppress aggregation, and except in QDs with very thick shells they are responsible for defining the electronic boundaries of the quantum well. In this study we used GPC purification to provide a well-defined initial state for association of neutral ligands to vacant sites. We have demonstrated that the decrease in QY observed on purification of QDs can be simply a result of ligand removal and is not necessarily due to irreversible changes or "damage" to the QD surface. Among the components of the CdSe-based core/shell samples tested here, the QY appears to be most critically affected by the loss of phosphine ligands on purification, because reintroduction of phosphine led to near-complete regeneration of QY with little change in absorption spectrum. In contrast, phosphine oxide and free carboxylic acid had a minimal effect on QY, and the primary amine showed significant QY regeneration only in the case of pure CdS shells. Introduction of Cd carboxylate equivalents led to a large increase in QY in a manner complementary to phosphine, but was also associated with irreversible structural changes.

Time-resolved PL allows us to conclude that the reduction and regeneration in QY are not experienced uniformly among the QDs in the ensemble, but are rather associated with the changes in the relative population between a subset with lifetime comparable to the radiative lifetime and a subset with significantly shorter lifetimes. A simple model of quenching by a binomially distributed number of recombination centers appears to be insufficient to describe the role of vacant sites in limiting QY.

We also show that ITC, a technique that does not require specific nuclei as spectroscopic probes or deuterated solvents, can be used to measure ligand interactions with QDs with nonzero molar enthalpy of binding. We expect ITC to become a versatile tool for studying ligand binding and interactions on nanoparticle surfaces. Due to its sensitivity, ITC does require a well-controlled reaction system, and it is important to identify purification methods and sample metrics that can ensure repeatable results for compound semiconductor nanocrystals.

METHODS AND MATERIALS

Materials. The following chemicals were used as received. Cadmium oxide (CdO; 99.999%), zinc oxide (ZnO; 99.999%), trioctylphosphine (TOP; 97%), and trioctylphosphine oxide (TOPO; 99%) were purchased from STREM Chemicals. Oleic acid (OA; 99%), 1-octadecene (ODE; 90% technical grade), and selenium (Se; 99.999%) were purchased from Alfa Aesar. 1-Tetradecylphosphonic acid (TDPA; >99%) was purchased from PCI Synthesis. Bio-Beads S-X1 GPC medium was obtained from Bio-Rad Laboratories. Toluene-d_8 (D, 99.5%) was obtained from Cambridge Isotope Laboratories. Decylamine (95%) was purchased from Sigma-Aldrich. Oleylamine (80−90%) and bis(trimethylsilyl) sulfide ($(TMS)_2S$; 95%) were purchased from Acros Organics. Rhodamine 590 chloride (R590, MW 464.98) was obtained from Exciton. Toluene (99.5%) and tetrahydrofuran (THF, 99%) were purchased from Mallinckrodt Chemicals. Ethyl alcohol (200 proof ethanol) was obtained from Decon Laboratories. Acetone (99.9%) was purchased from VWR. Methanol (99.9%) was purchased from Fisher Scientific. Toluene was dried with activated 4A molecular sieves. THF was dried using the Puresolv system from Innovative Technologies. Synthetic or analytical procedures under inert conditions were carried out using Schlenk line techniques, in a glovebox, under a N_2 atmosphere.

Optical Spectroscopy. The optical absorption spectrum was recorded using a Thermo Scientific Evolution Array UV−visible spectrophotometer with toluene as the solvent as well as the blank in a 1 cm path quartz cuvette. Routine emission spectra were recorded by an Ocean Optics USB 4000 spectrometer under ~365 nm excitation.

NMR Analysis of QDs. Routine NMR samples of the QDs were prepared in toluene-d_8. The QDs' concentration is set at approximately 20 μM; the exact value in each case was measured by UV−vis using the calculated molar extinction coefficient. The spectra were recorded on a Bruker Avance III 400. The quantitative ^{1}H NMR spectra were measured with ferrocene as the internal standard and 30 s relaxation delay, allowing the system to reach a reliable equilibrium. The ^{31}P NMR spectra of QD samples were measured with 512 scans to increase the signal-to-noise ratio. T_1 is measured by the vendor-supplied inversion recovery pulse sequence experiment. Diffusion measurements and NOE difference measurements on ^{1}H spectra with selective saturation on the ^{31}P resonance were performed with a Bruker Avance III HD 400 and analyzed by the Topspin version 3.2 software.

Synthesis of CdSe QDs. The CdSe cores were prepared by a hot-injection method[72] using cadmium tetradecylphosphonate as the Cd precursor, trioctylphosphine selenide as the Se precursor, and a mixture of TOP and TOPO as the solvent. The two precursors were mixed at high temperature (350 to 365 °C) and cooled with an air blower immediately after the injection. The lowest energy absorption peak for the CdSe cores used to prepare the CdSe/CdZnS samples was at 509 nm, while that of the CdSe cores used for the CdSe/CdS sample was at 522 nm.

CdZnS and CdS Overcoating. Shells were grown using a SILAR method described previously.[33,72] Briefly, a portion of as-synthesized CdSe cores was flocculated by methanol and acetone. After decanting the supernatant, the QDs were redissolved into hexane and stored in a freezer (−15 °C) for more than 12 h. All the undissolved materials were removed by centrifugation, and the sample was precipitated again by an addition of methanol and acetone. Afterward, the QDs were brought into a measured volume of hexane. The UV−vis absorption spectrum was recorded at a known dilution of the sample to determine the size and quantity of QDs. The solution of QDs in hexane was transferred to a solvent of 1:2 oleylamine/ODE (v/v, 9 mL total)

and degassed at 100 °C to remove hexane. Before the addition of the reagent *via* syringe pump, the system was heated to 200 °C under nitrogen. For the pure CdS shell growth, the Cd precursor is prepared by diluting 0.2 M $Cd(oleate)_2$ in ODE with 2 equiv of decylamine and a volume of TOP to yield a concentration of 0.1 M. For the CdZnS alloy shell growth, the metal precursor is prepared similarly to the pure Cd precursor but using a mixture of $Cd(oleate)_2$ and $Zn(oleate)_2$ (the ratio of Cd:Zn is 3:7) to yield a metal concentration of 0.1 M. The S precursor was always a 0.1 M solution of $(TMS)_2S$ in TOP. The volume increase associated with 1 monolayer coverage in both cases is calculated based on the radius increase of 3.37 Å, which is the half of the wurtzite *c*-axis unit cell dimensions for CdS. Alternating injections of metal precursor and sulfur precursor were performed, adding the metal precursor solution first, with injections starting every 15 min for the CdS shell and 20 min for the CdZnS shell. The flow rate was adjusted to complete each injection over the course of 3 min. The volume of each injection was calculated to apply 0.8 monolayer coverage each cycle (a cycle is defined as one metal precursor injection and one sulfur precursor injection). For the thin-shell samples (**CdSe/CdS_1** and **CdSe/CdZnS_1**), two cycles were performed, while five cycles were added to the thick-shell samples (**CdSe/CdS_2** and **CdSe/CdZnS_2**). The growth processes were monitored by both UV−vis absorption and fluorescence spectrometers. After the reaction, the mixture was cooled to room temperature and the molar extinction coefficient was estimated based on the amount of the core introduced at the beginning and the total volume of the solution after the synthesis.

Absolute Quantum Yield Measurement. The absolute QY of QD samples was assigned by comparison to a rhodamine 590 standard (R590, QY = 99% in ethanol).[77,97] Fluorescence spectra of QD and R590 dye were taken under identical spectrometer conditions on a Varian fluorescence spectrometer in triplicate and averaged. The optical density was kept below 0.1 from the excitation wavelength to 800 nm to avoid internal filtering effects. The QY was calculated based on the integrated intensities of the emission spectra, the absorption at the excitation wavelength, and the refraction index of the solvent using the equation

$$QY_{QDS} = QY_{dye}\frac{Absorbance_{dye}}{Absorbance_{QDS}} \times \frac{Emission\ integral_{QDS}}{Emission\ integral_{dye}} \times \frac{Refraction\ index^2_{toluene}}{Refraction\ index^2_{ethanol}}$$

The precision of this measurement in our case is limited by the precision of the absorbance measurement (∼1%), while the accuracy among samples in different solvents will be limited by the accuracy of the refractive index correction term.

GPC Purification of the QDs. The GPC column was packed as previously described[40] with toluene as the eluent. The as-synthesized core/shell QDs were purified by one cycle of precipitation with acetone only and redissolution in toluene. Then the QD solution was added to the column, and the sample was collected when the elution volume equaled ∼1/3 of the total volume of the column (the expected void volume for irregularly spaced spherical beads); this volume corresponds to the fraction at which the purified QDs eluted. The GPC column was rinsed thoroughly (3 times the total volume of the column) between runs.

Preparation of Pure Cd Oleate. The cadmium oleate used as a ligand in the regeneration study was prepared as follows. CdO and oleic acid were introduced to a three-neck flask (the ratio of CdO:OA is 1:5), where OA was used as both acid and solvent. The mixture was degassed and then heated to 270 °C under N_2 to form a colorless and clear solution. Then the sample was cooled and transferred to a refrigerator (4 °C) to allow the product to precipitate. Excess oleic acid was separated by filtration, and the insoluble $Cd(oleate)_2$ was washed with ethanol five times to remove the remaining oleic acid. FTIR and ^1H NMR have been used to confirm the removal of oleic acid (see Figure S15).

Quantum Yield Regeneration and Relative Quantum Yield Measurement. After GPC purification, the QD samples were transferred into a sealed N_2 environment and pumped into the glovebox immediately to avoid any possible oxidation. The ligand solutions are also prepared in the glovebox. For the regeneration process, the concentrations of the QD samples are fixed to be 0.5 μM and the ligand concentration is controlled to be 1.5 or 0.15 mM to provide two different ligand-to-QD ratios (3000:1 and 300:1, respectively). The total volume of the mixing solutions is 1 mL, and the solutions were kept gently stirring for the 7-day measurement period. The relative QY is characterized by diluting a portion of the above solutions into dry toluene and measuring the absorption and emission spectra. The optical densities of the sample solutions were kept below 0.1 at wavelengths above the 365 nm excitation wavelength to avoid internal filtering effects. The relative QY is calculated by comparing the integration of the emission spectrum divided by the absorption at 365 nm.

Time-Resolved Photoluminescence Measurement. The PL decays of QDs in toluene were collected in front-face mode with a 1 cm quartz cuvette in a lifetime spectrometer (Edinburgh Mini-τ) equipped with a 368 nm picosecond-pulsed light-emitting diode. A stirring stage was set under the Mini-τ, and a mini stirring bar was placed in the cuvette to stir the QD solution to avoid accumulation of photoproducts during the measurement. The instrument response function was recorded using Rayleigh scattering of pure water.

Reversibility Test. QD samples are purified by GPC and mixed with 3000 equiv of ligand. After stirring inside the glovebox for 1 day, the mixtures were purified again by GPC. Absorption and emission spectra were monitored during the process.

Inductively Coupled Plasma-Mass Spectrometry Analysis. Two samples were prepared. One was made by diluting 1 nmol of GPC-purified **CdSe/CdZnS_1** QDs in 0.5 mL of toluene; the other by mixing 1 nmol of the same QD sample with 3 μmol of CdOA (3000:1 ratio) in 0.5 mL of toluene. After stirring under N_2 overnight, these two samples were precipitated by acetone and the supernatants were transferred and evacuated to dryness. Aqua regia (1 mL) was introduced and was allowed to digest the sample for 2 h. Then the solutions were brought to 50 mL in a volumetric flask with 2% HNO_3 in water. The concentrations of Zn were detected by a Thermo-Finnigan Element XR ICP-MS.

Isothermal Titration Calorimetry. Isothermal titration calorimetry experiments were performed on a VP-ITC calorimeter (Microcal Inc., Northampton, MA, USA). Ligand solutions were titrated from the 300 μL injection syringe to the sample cell loaded to its 1.8 mL filling capacity, and the heat response to maintain a constant temperature between the sample cell and reference was monitored. The sample cell was purged with nitrogen before loading the GPC-purified QD solution to minimize the influence of the oxidation reactions. Each experiment was conducted at 22 °C and midrange reference power and allowed to equilibrate prior to an initial 600 s delay, and in order to allow adequate equilibration between each injection, 8−9 min intervals were set between each injection for a total of 60 injections in 5 μL increments. Dry THF was chosen as the solvent for both the ligands and QDs, as well as the blank solvent in the reference cell. Reference titrations were conducted to determine any significant heat of dilution between the solvent, ligand solution, and QD solutions that may have accounted for signal in the final ligand−QD titrations. Only ligand−solvent reference titrations were subtracted from ligand−QD titrations, as other reference titrations were determined to be negligible. The QD solutions loaded in the sample cell were 0.5 μM (same as for QY regeneration), and ligand solutions loaded in the syringe were 1.5 mM.

Conflict of Interest: The authors declare no competing financial interest.

Supporting Information Available: Supplementary figures and tables, including PL decay analysis and NMR results. This material is available free of charge *via* the Internet at http://pubs.acs.org.

Acknowledgment. This research was supported by the University of South Carolina, including a SPARC Graduate Research Fellowship to Y.S. and a College of Arts and Sciences Small Research Instrumentation Grant supporting time-resolved

photoluminescence. Additional support was provided through South Carolina EPSCOR grant EPS-0903795, a subaward from NSF-1317771. We thank M. Chruszcz, Q. Wang, and R. Adams for use of equipment for calorimetry and spectroscopy, P.J. Pellechia for assistance with NMR spectroscopy, and L. Lovelace, N. Mank, and B. Lever for helpful discussions. We also thank A. Roberge for assistance in preparing the TOC image.

REFERENCES AND NOTES

1. Smith, A. M.; Nie, S. Semiconductor Nanocrystals: Structure, Properties, and Band Gap Engineering. *Acc. Chem. Res.* **2010**, *43*, 190–200.
2. Leatherdale, C. A.; Woo, W.-K.; Mikulec, F. V.; Bawendi, M. G. On the Absorption Cross Section of CdSe Nanocrystal Quantum Dots. *J. Phys. Chem. B* **2002**, *106*, 7619–7622.
3. Jasieniak, J.; Smith, L.; Embden, J.; van Mulvaney, P.; Califano, M. Re-Examination of the Size-Dependent Absorption Properties of CdSe Quantum Dots. *J. Phys. Chem. C* **2009**, *113*, 19468–19474.
4. Blanton, S. A.; Hines, M. A.; Schmidt, M. E.; Guyot-Sionnest, P. Two-Photon Spectroscopy and Microscopy of II-VI Semiconductor Nanocrystals. *J. Lumin.* **1996**, *70*, 253–268.
5. Larson, D. R.; Zipfel, W. R.; Williams, R. M.; Clark, S. W.; Bruchez, M. P.; Wise, F. W.; Webb, W. W. Water-Soluble Quantum Dots for Multiphoton Fluorescence Imaging *in Vivo*. *Science* **2003**, *300*, 1434–1436.
6. Wu, X.; Liu, H.; Liu, J.; Haley, K. N.; Treadway, J. A.; Larson, J. P.; Ge, N.; Peale, F.; Bruchez, M. P. Immunofluorescent Labeling of Cancer Marker Her2 and Other Cellular Targets with Semiconductor Quantum Dots. *Nat. Biotechnol.* **2003**, *21*, 41–46.
7. Medintz, I. L.; Uyeda, H. T.; Goldman, E. R.; Mattoussi, H. Quantum Dot Bioconjugates for Imaging, Labelling and Sensing. *Nat. Mater.* **2005**, *4*, 435–446.
8. Erathodiyil, N.; Ying, J. Y. Functionalization of Inorganic Nanoparticles for Bioimaging Applications. *Acc. Chem. Res.* **2011**, *44*, 925–935.
9. Lemon, C. M.; Curtin, P. N.; Somers, R. C.; Greytak, A. B.; Lanning, R. M.; Jain, R. K.; Bawendi, M. G.; Nocera, D. G. Metabolic Tumor Profiling with pH, Oxygen, and Glucose Chemosensors on a Quantum Dot Scaffold. *Inorg. Chem.* **2014**, *53*, 1900–1915.
10. Zhang, B.; Hu, R.; Wang, Y.; Yang, C.; Liu, X.; Yong, K.-T. Revisiting the Principles of Preparing Aqueous Quantum Dots for Biological Applications: The Effects of Surface Ligands on the Physicochemical Properties of Quantum Dots. *RSC Adv.* **2014**, *4*, 13805–13816.
11. Anikeeva, P. O.; Halpert, J. E.; Bawendi, M. G.; Bulović, V. Quantum Dot Light-Emitting Devices with Electroluminescence Tunable over the Entire Visible Spectrum. *Nano Lett.* **2009**, *9*, 2532–2536.
12. Talapin, D. V.; Lee, J.-S.; Kovalenko, M. V.; Shevchenko, E. V. Prospects of Colloidal Nanocrystals for Electronic and Optoelectronic Applications. *Chem. Rev.* **2010**, *110*, 389–458.
13. Panthani, M. G.; Kurley, J. M.; Crisp, R. W.; Dietz, T. C.; Ezzyat, T.; Luther, J. M.; Talapin, D. V. High Efficiency Solution Processed Sintered CdTe Nanocrystal Solar Cells: The Role of Interfaces. *Nano Lett.* **2014**, *14*, 670–675.
14. Zhang, J.; Gao, J.; Miller, E. M.; Luther, J. M.; Beard, M. C. Diffusion-Controlled Synthesis of PbS and PbSe Quantum Dots with *in Situ* Halide Passivation for Quantum Dot Solar Cells. *ACS Nano* **2014**, *8*, 614–622.
15. Zhitomirsky, D.; Voznyy, O.; Levina, L.; Hoogland, S.; Kemp, K. W.; Ip, A. H.; Thon, S. M.; Sargent, E. H. Engineering Colloidal Quantum Dot Solids within and beyond the Mobility-Invariant Regime. *Nat. Commun.* **2014**, *5*, 3803.
16. Meinardi, F.; Colombo, A.; Velizhanin, K. A.; Simonutti, R.; Lorenzon, M.; Beverina, L.; Viswanatha, R.; Klimov, V. I.; Brovelli, S. Large-Area Luminescent Solar Concentrators Based on Stokes-Shift-Engineered Nanocrystals in a Mass-Polymerized PMMA Matrix. *Nat. Photonics* **2014**, *8*, 392–399.
17. Erickson, C. S.; Bradshaw, L. R.; McDowall, S.; Gilbertson, J. D.; Gamelin, D. R.; Patrick, D. L. Zero-Reabsorption Doped-Nanocrystal Luminescent Solar Concentrators. *ACS Nano* **2014**, *8*, 3461–3467.
18. Geyer, S. M.; Scherer, J. M.; Moloto, N.; Jaworski, F. B.; Bawendi, M. G. Efficient Luminescent Down-Shifting Detectors Based on Colloidal Quantum Dots for Dual-Band Detection Applications. *ACS Nano* **2011**, *5*, 5566–5571.
19. Zhu, H.; Yang, Y.; Lian, T. Multiexciton Annihilation and Dissociation in Quantum Confined Semiconductor Nanocrystals. *Acc. Chem. Res.* **2013**, *46*, 1270–1279.
20. Efros, A. L.; Rosen, M. Random Telegraph Signal in the Photoluminescence Intensity of a Single Quantum Dot. *Phys. Rev. Lett.* **1997**, *78*, 1110.
21. Frantsuzov, P. A.; Volkán-Kacsó, S.; Jankó, B. Model of Fluorescence Intermittency of Single Colloidal Semiconductor Quantum Dots Using Multiple Recombination Centers. *Phys. Rev. Lett.* **2009**, *103*, 207402.
22. Chen, Y.; Vela, J.; Htoon, H.; Casson, J. L.; Werder, D. J.; Bussian, D. A.; Klimov, V. I.; Hollingsworth, J. A. Giant Multishell CdSe Nanocrystal Quantum Dots with Suppressed Blinking. *J. Am. Chem. Soc.* **2008**, *130*, 5026–5027.
23. Mahler, B.; Spinicelli, P.; Buil, S.; Quelin, X.; Hermier, J.-P.; Dubertret, B. Towards Non-Blinking Colloidal Quantum Dots. *Nat. Mater.* **2008**, *7*, 659–664.
24. Spinicelli, P.; Buil, S.; Quelin, X.; Mahler, B.; Dubertret, B.; Hermier, J.-P. Bright and Grey States in CdSe-CdS Nanocrystals Exhibiting Strongly Reduced Blinking. *Phys. Rev. Lett.* **2009**, *102*, 136801.
25. Efros, A. L.; Rosen, M.; Kuno, M.; Nirmal, M.; Norris, D. J.; Bawendi, M. Band-Edge Exciton in Quantum Dots of Semiconductors with a Degenerate Valence Band: Dark and Bright Exciton States. *Phys. Rev. B* **1996**, *54*, 4843–4856.
26. Schlegel, G.; Bohnenberger, J.; Potapova, I.; Mews, A. Fluorescence Decay Time of Single Semiconductor Nanocrystals. *Phys. Rev. Lett.* **2002**, *88*, 137401.
27. Fisher, B. R.; Eisler, H. J.; Stott, N. E.; Bawendi, M. G. Emission Intensity Dependence and Single-Exponential Behavior in Single Colloidal Quantum Dot Fluorescence Lifetimes. *J. Phys. Chem. B* **2004**, *108*, 143–148.
28. Kuno, M.; Lee, J. K.; Dabbousi, B. O.; Mikulec, F. V.; Bawendi, M. G. The Band Edge Luminescence of Surface Modified CdSe Nanocrystallites: Probing the Luminescing State. *J. Chem. Phys.* **1997**, *106*, 9869–9882.
29. Mooney, J.; Krause, M. M.; Saari, J. I.; Kambhampati, P. A Microscopic Picture of Surface Charge Trapping in Semiconductor Nanocrystals. *J. Chem. Phys.* **2013**, *138*, 204705.
30. Kalyuzhny, G.; Murray, R. W. Ligand Effects on Optical Properties of CdSe Nanocrystals. *J. Phys. Chem. B* **2005**, *109*, 7012–7021.
31. Bullen, C.; Mulvaney, P. The Effects of Chemisorption on the Luminescence of CdSe Quantum Dots. *Langmuir* **2006**, *22*, 3007–3013.
32. Munro, A. M.; Ginger, D. S. Photoluminescence Quenching of Single CdSe Nanocrystals by Ligand Adsorption. *Nano Lett.* **2008**, *8*, 2585–2590.
33. Greytak, A. B.; Allen, P. M.; Liu, W.; Zhao, J.; Young, E. R.; Popović, Z.; Walker, B. J.; Nocera, D. G.; Bawendi, M. G. Alternating Layer Addition Approach to CdSe/CdS Core/Shell Quantum Dots with near-Unity Quantum Yield and High On-Time Fractions. *Chem. Sci.* **2012**, *3*, 2028–2034.
34. Anderson, N. C.; Owen, J. S. Soluble, Chloride-Terminated CdSe Nanocrystals: Ligand Exchange Monitored by ^{1}H and ^{31}P NMR Spectroscopy. *Chem. Mater.* **2013**, *25*, 69–76.
35. Peterson, M. D.; Cass, L. C.; Harris, R. D.; Edme, K.; Sung, K.; Weiss, E. A. The Role of Ligands in Determining the Exciton Relaxation Dynamics in Semiconductor Quantum Dots. *Annu. Rev. Phys. Chem.* **2014**, *65*, 317–339.
36. Hines, M. A.; Guyot-Sionnest, P. Synthesis and Characterization of Strongly Luminescing ZnS-Capped CdSe Nanocrystals. *J. Phys. Chem.* **1996**, *100*, 468–471.
37. Qin, H.; Niu, Y.; Meng, R.; Lin, X.; Lai, R.; Fang, W.; Peng, X. Single-Dot Spectroscopy of Zinc-Blende CdSe/CdS Core/Shell Nanocrystals: Nonblinking and Correlation with Ensemble Measurements. *J. Am. Chem. Soc.* **2013**, *136*, 179–187.

38. Morris-Cohen, A. J.; Malicki, M.; Peterson, M. D.; Slavin, J. W. J.; Weiss, E. A. Chemical, Structural, and Quantitative Analysis of the Ligand Shells of Colloidal Quantum Dots. *Chem. Mater.* **2013**, *25*, 1155–1165.
39. Liu, W.; Howarth, M.; Greytak, A. B.; Zheng, Y.; Nocera, D. G.; Ting, A. Y.; Bawendi, M. G. Compact Biocompatible Quantum Dots Functionalized for Cellular Imaging. *J. Am. Chem. Soc.* **2008**, *130*, 1274–1284.
40. Shen, Y.; Gee, M. Y.; Tan, R.; Pellechia, P. J.; Greytak, A. B. Purification of Quantum Dots by Gel Permeation Chromatography and the Effect of Excess Ligands on Shell Growth and Ligand Exchange. *Chem. Mater.* **2013**, *25*, 2838–2848.
41. Morris-Cohen, A. J.; Donakowski, M. D.; Knowles, K. E.; Weiss, E. A. The Effect of a Common Purification Procedure on the Chemical Composition of the Surfaces of CdSe Quantum Dots Synthesized with Trioctylphosphine Oxide. *J. Phys. Chem. C* **2010**, *114*, 897–906.
42. Hassinen, A.; Moreels, I.; De Nolf, K.; Smet, P. F.; Martins, J. C.; Hens, Z. Short-Chain Alcohols Strip X-Type Ligands and Quench the Luminescence of PbSe and CdSe Quantum Dots, Acetonitrile Does Not. *J. Am. Chem. Soc.* **2012**, *134*, 20705–20712.
43. Owen, J. The Coordination Chemistry of Nanocrystal Surfaces. *Science* **2015**, *347*, 615–616.
44. Guyot-Sionnest, P.; Wehrenberg, B.; Yu, D. Intraband Relaxation in CdSe Nanocrystals and the Strong Influence of the Surface Ligands. *J. Chem. Phys.* **2005**, *123*, 074709.
45. McArthur, E. A.; Morris-Cohen, A. J.; Knowles, K. E.; Weiss, E. A. Charge Carrier Resolved Relaxation of the First Excitonic State in CdSe Quantum Dots Probed with Near-Infrared Transient Absorption Spectroscopy. *J. Phys. Chem. B* **2009**, *114*, 14514–14520.
46. Kilina, S.; Velizhanin, K. A.; Ivanov, S.; Prezhdo, O. V.; Tretiak, S. Surface Ligands Increase Photoexcitation Relaxation Rates in CdSe Quantum Dots. *ACS Nano* **2012**, *6*, 6515–6524.
47. Munro, A. M.; Jen-La Plante, I.; Ng, M. S.; Ginger, D. S. Quantitative Study of the Effects of Surface Ligand Concentration on CdSe Nanocrystal Photoluminescence. *J. Phys. Chem. C* **2007**, *111*, 6220–6227.
48. Knowles, K. E.; Tice, D. B.; McArthur, E. A.; Solomon, G. C.; Weiss, E. A. Chemical Control of the Photoluminescence of CdSe Quantum Dot−Organic Complexes with a Series of Para-Substituted Aniline Ligands. *J. Am. Chem. Soc.* **2009**, *132*, 1041–1050.
49. Morris-Cohen, A. J.; Vasilenko, V.; Amin, V. A.; Reuter, M. G.; Weiss, E. A. Model for Adsorption of Ligands to Colloidal Quantum Dots with Concentration-Dependent Surface Structure. *ACS Nano* **2012**, *6*, 557–565.
50. Zhu, H.; Song, N.; Lian, T. Wave Function Engineering for Ultrafast Charge Separation and Slow Charge Recombination in Type II Core/Shell Quantum Dots. *J. Am. Chem. Soc.* **2011**, *133*, 8762–8771.
51. Zhao, H.; Chaker, M.; Ma, D. Self-Selective Recovery of Photoluminescence in Amphiphilic Polymer Encapsulated PbS Quantum Dots. *Phys. Chem. Chem. Phys.* **2010**, *12*, 14754–14761.
52. Lee, J. R. I.; Whitley, H. D.; Meulenberg, R. W.; Wolcott, A.; Zhang, J. Z.; Prendergast, D.; Lovingood, D. D.; Strouse, G. F.; Ogitsu, T.; Schwegler, E.; Terminello, L. J.; van Buuren, T. Ligand-Mediated Modification of the Electronic Structure of CdSe Quantum Dots. *Nano Lett.* **2012**, *12*, 2763–2767.
53. Anderson, N. C.; Hendricks, M. P.; Choi, J. J.; Owen, J. S. Ligand Exchange and the Stoichiometry of Metal Chalcogenide Nanocrystals: Spectroscopic Observation of Facile Metal-Carboxylate Displacement and Binding. *J. Am. Chem. Soc.* **2013**, *135*, 18536–18548.
54. Ji, X.; Copenhaver, D.; Sichmeller, C.; Peng, X. Ligand Bonding and Dynamics on Colloidal Nanocrystals at Room Temperature: The Case of Alkylamines on CdSe Nanocrystals. *J. Am. Chem. Soc.* **2008**, *130*, 5726–5735.
55. Williams, E. S.; Major, K. J.; Tobias, A.; Woodall, D.; Morales, V.; Lippincott, C.; Moyer, P. J.; Jones, M. Characterizing the Influence of TOPO on Exciton Recombination Dynamics in Colloidal CdSe Quantum Dots. *J. Phys. Chem. C* **2013**, *117*, 4227–4237.
56. Yang, J.; Yang, P. Photoluminescent Enhancement of CdSe/Cd1−x Zn X S Quantum Dots by Hexadecylamine at Room Temperature. *J. Nanosci. Nanotechnol.* **2012**, *12*, 7322–7328.
57. Park, C.; Yoon, T. H. L-Cysteine-Induced Photoluminescence Enhancement of CdSe/ZnSe Quantum Dots in Aqueous Solution. *Colloids Surf. B Biointerfaces* **2010**, *75*, 472–477.
58. Chen, C.-J.; Chiang, R.-K.; Huang, C.-Y.; Lien, J.-Y.; Wang, S.-L. Thiol Treatment to Enhance Photoluminescence and Electroluminescence of CdSe/CdS Core−Shell Quantum Dots Prepared by Thermal Cycling of Single Source Precursors. *RSC Adv.* **2015**, *5*, 9819–9827.
59. Wang, M.; Zhang, M.; Qian, J.; Zhao, F.; Shen, L.; Scholes, G. D.; Winnik, M. A. Enhancing the Photoluminescence of Polymer-Stabilized CdSe/CdS/ZnS Core/Shell/Shell and CdSe/ZnS Core/Shell Quantum Dots in Water through a Chemical-Activation Approach. *Langmuir* **2009**, *25*, 11732–11740.
60. Oszajca, M.; Lincheneau, C.; Amelia, M.; Schäfer, C.; Szaciłowski, K.; Credi, A. Photoluminescence Enhancement of CdSe and CdSe−ZnS Nanocrystals by on-Surface Ligand Modification. *Eur. J. Inorg. Chem.* **2013**, *2013*, 3550–3556.
61. Sharma, S. N.; Pillai, Z. S.; Kamat, P. V. Photoinduced Charge Transfer between CdSe Quantum Dots and P-Phenylenediamine. *J. Phys. Chem. B* **2003**, *107*, 10088–10093.
62. Burda, C.; Link, S.; Mohamed, M.; El-Sayed, M. The Relaxation Pathways of CdSe Nanoparticles Monitored with Femtosecond Time-Resolution from the Visible to the IR: Assignment of the Transient Features by Carrier Quenching. *J. Phys. Chem. B* **2001**, *105*, 12286–12292.
63. Kern, S. J.; Sahu, K.; Berg, M. A. Heterogeneity of the Electron-Trapping Kinetics in CdSe Nanoparticles. *Nano Lett.* **2011**, *11*, 3493–3498.
64. Jones, M.; Lo, S. S.; Scholes, G. D. Quantitative Modeling of the Role of Surface Traps in CdSe/CdS/ZnS Nanocrystal Photoluminescence Decay Dynamics. *Proc. Natl. Acad. Sci. U.S.A.* **2009**, *106*, 3011–3016.
65. Zhao, J.; Nair, G.; Fisher, B. R.; Bawendi, M. G. Challenge to the Charging Model of Semiconductor-Nanocrystal Fluorescence Intermittency from Off-State Quantum Yields and Multiexciton Blinking. *Phys. Rev. Lett.* **2010**, *104*, 157403.
66. Hens, Z.; Martins, J. C. A Solution NMR Toolbox for Characterizing the Surface Chemistry of Colloidal Nanocrystals. *Chem. Mater.* **2013**, *25*, 1211–1221.
67. Freyer, M. W.; Lewis, E. A. Isothermal Titration Calorimetry: Experimental Design, Data Analysis, and Probing Macromolecule/Ligand Binding and Kinetic Interactions. *Methods Cell Biol.* **2008**, *84*, 79–113.
68. Grossoehme, N.; Spuches, A.; Wilcox, D. Application of Isothermal Titration Calorimetry in Bioinorganic Chemistry. *J. Biol. Inorg. Chem.* **2010**, *15*, 1183–1191.
69. Ravi, V.; Binz, J. M.; Rioux, R. M. Thermodynamic Profiles at the Solvated Inorganic-Organic Interface: The Case of Gold-Thiolate Monolayers. *Nano Lett.* **2013**, *13*, 4442–4448.
70. Lindman, S.; Lynch, I.; Thulin, E.; Nilsson, H.; Dawson, K. A.; Linse, S. Systematic Investigation of the Thermodynamics of HSA Adsorption to N-Iso-Propylacrylamide/N-Tert-Butylacrylamide Copolymer Nanoparticles. Effects of Particle Size and Hydrophobicity. *Nano Lett.* **2007**, *7*, 914–920.
71. Mondal, S.; Ghosh, S.; Ghosh, D.; Saha, A. Physico-Chemical Aspects of Quantum Dot−Vasodialator Interaction: Implications in Nanodiagnostics. *J. Phys. Chem. C* **2012**, *116*, 9774–9782.
72. Tan, R.; Blom, D. A.; Ma, S.; Greytak, A. B. Probing Surface Saturation Conditions in Alternating Layer Growth of CdSe/CdS Core/Shell Quantum Dots. *Chem. Mater.* **2013**, *25*, 3724–3736.
73. Li, J. J.; Wang, Y. A.; Guo, W. Z.; Keay, J. C.; Mishima, T. D.; Johnson, M. B.; Peng, X. G. Large-Scale Synthesis of Nearly Monodisperse CdSe/CdS Core/Shell Nanocrystals Using Air-Stable Reagents *via* Successive Ion Layer Adsorption and Reaction. *J. Am. Chem. Soc.* **2003**, *125*, 12567–12575.

74. Davis, K.; Qi, B.; Witmer, M.; Kitchens, C. L.; Powell, B. A.; Mefford, O. T. Quantitative Measurement of Ligand Exchange on Iron Oxides *via* Radiolabeled Oleic Acid. *Langmuir* **2014**, *30*, 10918–10925.
75. Owen, J. S.; Park, J.; Trudeau, P.-E.; Alivisatos, A. P. Reaction Chemistry and Ligand Exchange at Cadmium−Selenide Nanocrystal Surfaces. *J. Am. Chem. Soc.* **2008**, *130*, 12279–12281.
76. Kopping, J. T.; Patten, T. E. Identification of Acidic Phosphorus-Containing Ligands Involved in the Surface Chemistry of CdSe Nanoparticles Prepared in Tri-N-Octylphosphine Oxide Solvents. *J. Am. Chem. Soc.* **2008**, *130*, 5689–5698.
77. Beaumont, P. C.; Johnson, D. G.; Parsons, B. J. Photophysical Properties of Laser Dyes: Picosecond Laser Flash Photolysis Studies of Rhodamine 6G, Rhodamine B and Rhodamine 101. *J. Chem. Soc. Faraday Trans.* **1993**, *89*, 4185.
78. Gomes, R.; Hassinen, A.; Szczygiel, A.; Zhao, Q.; Vantomme, A.; Martins, J. C.; Hens, Z. Binding of Phosphonic Acids to CdSe Quantum Dots: A Solution NMR Study. *J. Phys. Chem. Lett.* **2011**, *2*, 145–152.
79. Knowles, K. E.; Frederick, M. T.; Tice, D. B.; Morris-Cohen, A. J.; Weiss, E. A. Colloidal Quantum Dots: Think Outside the (Particle-in-a-)Box. *J. Phys. Chem. Lett.* **2012**, *3*, 18–26.
80. Ning, Z.; Molnar, M.; Chen, Y.; Friberg, P.; Gan, L.; Agren, H.; Fu, Y. Role of Surface Ligands in Optical Properties of Colloidal CdSe/CdS Quantum Dots. *Phys. Chem. Chem. Phys.* **2011**, *13*, 5848–5854.
81. Jasieniak, J.; Mulvaney, P. From Cd-Rich to Se-Rich − the Manipulation of CdSe Nanocrystal Surface Stoichiometry. *J. Am. Chem. Soc.* **2007**, *129*, 2841–2848.
82. Minotto, A.; Todescato, F.; Fortunati, I.; Signorini, R.; Jasieniak, J. J.; Bozio, R. Role of Core−Shell Interfaces on Exciton Recombination in CdSe-$Cd_xZn_{1-x}S$ Quantum Dots. *J. Phys. Chem. C* **2014**, *118*, 24117–24126.
83. Lakowicz, J. R. *Principles of Fluorescence Spectroscopy*, 3rd ed.; Springer: New York, 2006.
84. Sillen, A.; Engelborghs, Y. The Correct Use of "Average" Fluorescence Parameters. *Photochem. Photobiol.* **1998**, *67*, 475–486.
85. Galland, C.; Ghosh, Y.; Steinbrück, A.; Sykora, M.; Hollingsworth, J. A.; Klimov, V. I.; Htoon, H. Two Types of Luminescence Blinking Revealed by Spectroelectrochemistry of Single Quantum Dots. *Nature* **2011**, *479*, 203–207.
86. Orfield, N. J.; McBride, J. R.; Keene, J. D.; Davis, L. M.; Rosenthal, S. J. Correlation of Atomic Structure and Photoluminescence of the Same Quantum Dot: Pinpointing Surface and Internal Defects That Inhibit Photoluminescence. *ACS Nano* **2014**, *9*, 831–839.
87. Tyagi, P.; Kambhampati, P. False Multiple Exciton Recombination and Multiple Exciton Generation Signals in Semiconductor Quantum Dots Arise from Surface Charge Trapping. *J. Chem. Phys.* **2011**, *134*, 094706.
88. Singh, G.; Guericke, M. A.; Song, Q.; Jones, M. A Multipulse Time-Resolved Fluorescence Method for Probing Second-Order Recombination Dynamics in Colloidal Quantum Dots. *J. Phys. Chem. C* **2014**, *118*, 14692–14702.
89. Son, D. H.; Hughes, S. M.; Yin, Y. D.; Alivisatos, A. P. Cation Exchange Reactions-in Ionic Nanocrystals. *Science* **2004**, *306*, 1009–1012.
90. Lambert, K.; Geyter, B. D.; Moreels, I.; Hens, Z. PbTe|CdTe Core|Shell Particles by Cation Exchange, a HR-TEM Study. *Chem. Mater.* **2009**, *21*, 778–780.
91. Li, H.; Zanella, M.; Genovese, A.; Povia, M.; Falqui, A.; Giannini, C.; Manna, L. Sequential Cation Exchange in Nanocrystals: Preservation of Crystal Phase and Formation of Metastable Phases. *Nano Lett.* **2011**, *11*, 4964–4970.
92. Ren, L.; Hardy, C. G.; Tang, S.; Doxie, D. B.; Hamidi, N.; Tang, C. Preparation of Side-Chain 18-E Cobaltocenium-Containing Acrylate Monomers and Polymers. *Macromolecules* **2010**, *43*, 9304–9310.
93. Hassinen, A.; Moreels, I.; de Mello Donegá, C.; Martins, J. C.; Hens, Z. Nuclear Magnetic Resonance Spectroscopy Demonstrating Dynamic Stabilization of CdSe Quantum Dots by Alkylamines. *J. Phys. Chem. Lett.* **2010**, *1*, 2577–2581.
94. Fleischer, C. C.; Payne, C. K. Secondary Structure of Corona Proteins Determines the Cell Surface Receptors Used by Nanoparticles. *J. Phys. Chem. B* **2014**, *118*, 14017–14026.
95. Rempel, J. Y.; Trout, B. L.; Bawendi, M. G.; Jensen, K. F. Density Functional Theory Study of Ligand Binding on CdSe (0001), (000$\bar{1}$), and (11$\bar{2}$0) Single Crystal Relaxed and Reconstructed Surfaces: Implications for Nanocrystalline Growth. *J. Phys. Chem. B* **2006**, *110*, 18007–18016.
96. Shanavas, K. V.; Sharma, S. M.; Dasgupta, I.; Nag, A.; Hazarika, A.; Sarma, D. D. First-Principles Study of the Effect of Organic Ligands on the Crystal Structure of CdS Nanoparticles. *J. Phys. Chem. C* **2012**, *116*, 6507–6511.
97. Grabolle, M.; Spieles, M.; Lesnyak, V.; Gaponik, N.; Eychmüller, A.; Resch-Genger, U. Determination of the Fluorescence Quantum Yield of Quantum Dots: Suitable Procedures and Achievable Uncertainties. *Anal. Chem.* **2009**, *81*, 6285–6294.